metals

MDPI

Article

Influence of Al on Evolution of the Inclusions in Ti-Bearing Steel with Ca Treatment

Yandong Li [1], Tongsheng Zhang [2,*] and Huamei Duan [3]

[1] College of Materials Science and Engineering, Yangtze Normal University, Chongqing 408000, China; andyydlee@gmail.com
[2] School of Metallurgy and Environment, Central South University, Changsha 410083, China
[3] College of Materials Science and Engineering, Chongqing University, Chongqing 400044, China; duanhuamei@cqu.edu.cn
* Correspondence: tongsheng.zhang@csu.edu.cn; Tel.: +86-139-7498-2473

Received: 29 December 2018; Accepted: 18 January 2019; Published: 21 January 2019

Abstract: Experimental simulations of steelmaking with different amounts of aluminum were achieved in the tube furnace at 1873 K and field scanning electron microscopy and energy dispersive X-ray spectroscopy (FE-SEM and EDX) were employed to explore the characteristics of the inclusions in Ti-bearing steel during the calcium treatment process. It was found that morphologies, chemical compositions, and the size distribution of the inclusions were obviously different before and after calcium treatment. The calcium addition need be carefully considered regarding the mass fraction of aluminum with the purpose of modifying the solid inclusions to liquid phases. The thermodynamic analysis of inclusion formation in the Al–Ti–Ca–O system at 1873 K was conducted, as well as transformation behaviors of inclusions including all types of solid inclusions and liquid phases during solidification. The thermodynamic equilibrium calculations are in good agreement with experimental data, which can be used to estimate inclusion formation in Ti-bearing steel.

Keywords: deoxidation; inclusions; thermodynamics; Ti-bearing steel; Ca treatment

1. Introduction

The quality of steel products can be effectively increased after being treated with the element titanium [1–4]. Titanium oxides and titanium carbides can be generated during the deoxidation process, which can promote the mechanical properties around the region of welded steels by improving the nucleation ratio of intragranular bainite [5–9]. However, TiO_x inclusions have a high probability of being agglomerate and subsequently form clusters, which results in the serious clogging issue of submerged entry nozzle and, consequently, lower the productivity of the continuous casting process as well [9–11]. Owing to the importance of Ti-containing inclusions, scholars have conducted a number of studies on inclusion control in Ti-bearing Al-killed steel, such as on thermodynamic computation and analysis [12–22], size distribution statistics [23–26], precipitation mechanisms [10,11,16,20], reaction kinetics, and evolution trajectory [14], mostly within the alumina and titanate system. In other words, it is usually difficult to keep the Al–Ti–O system inclusions as liquid phases during the production process at the present period.

It is generally the technique of calcium treatment that has been introduced to get liquid phases of calcium aluminate at casting temperature, which relieves the nozzle clogging issue during continuous process of steels, especially of grades of Al-killed steel, and also has benefits for the mechanical performance of final steel products [27–37]. However, the research involving the calcium treatment process of Ti-bearing Al-killed steel have been limited, until now [38–42]. In addition, the types of

inclusions at the solidification temperature are directly related to the properties of the inclusions in the final product.

In this work, the laboratory-scale melts, with different mass fractions of calcium and aluminum, were prepared in order to clarify the influence of aluminum element on inclusion properties during the calcium treatment process of Ti-bearing Al-killed steels. Then, FE-SEM and EDX were employed to observe and analyze morphologies, chemical compositions, and number and size of inclusions in steel cylinder sampled from high-temperature melts before and after calcium treatment. In addition, equilibrium phases of inclusions at smelting temperature were calculated, and the transformation behaviors of inclusions during the process of solidification were estimated by the commercial software FactSage. Present works will lay the experimental and thermodynamic foundation on expanding the combined treatment of titanium and calcium to industrial-scale production, and suggest an alternative way to eliminate the nozzle clogging issue during the continuous casting process of Ti-bearing Al-killed steel.

2. Experimental Methods

Three sets of experiments were conducted in the furnace according to the schematic diagram shown in Figure 1. A 350 gram plate of iron was loaded in the Al_2O_3 crucible surrounded by the graphite crucible, and then the graphite crucible was placed into the furnace which was heated to 1873 K in the protective atmosphere of high-purity argon gas with a constant flow rate. Thereafter, the furnace temperature was maintained for 0.5 h after the raw materials were completely melted at 1873 K to reach the full homogenization of solutes. At the time node of before and after deoxidant (Al and Ti) addition, the activity of dissolve oxygen was determined by the oxygen probe with a resolution of $\pm 10^{-6}$. The cylinder steel sample was extracted by the quartz tube with the inner diameter of 3 millimeters, and then immediately quenched into water at ambient temperature. At last, Ca treatment was carried out by adding Ca–Fe alloy. Another steel sample was obtained in the above way just 10 min after Ca treatment. The experimental details are shown in Figure 2, and the compositions of the raw materials in the work involving ARMCO iron, Ca–Fe alloy, and Al wire are listed in Table 1.

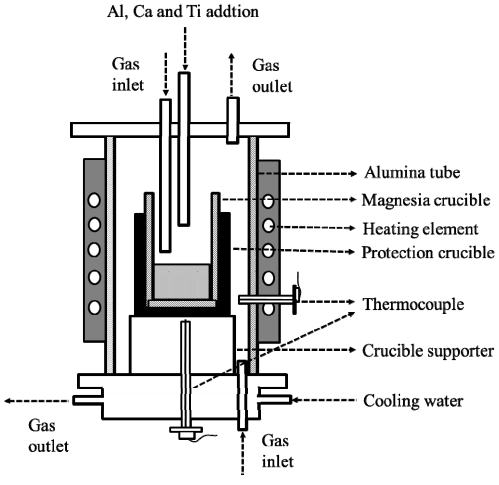

Figure 1. The schematic diagram of the experimental set-up.

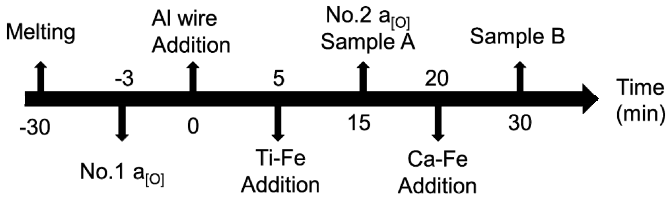

Figure 2. The melting sequence of experiment process and sampling.

Table 1. The compositions of experimental materials (mass %).

Type	Fe	C	Ti	Mn	Si	Ca	Al	P	S	Others
Ca–Fe alloy	69.82	-	-	-	-	30.10	-	-	-	0.08
Ti–Fe alloy	26.513	0.130	69.594	0.241	0.030	-	3.192	0.025	0.011	0.284
Al wire	-	-	-	-	-	-	99.99	-	-	0.01
Pure iron	99.944	0.002	-	0.03	0.01	-	0.001	0.007	0.007	0.043

The obtained steel samples were machined to two cylinders. One was adopted to analyze the chemical compositions by inductively coupled plasma-optical emission spectroscopy (ICP-OES) (Thermo Fisher Scientific ICAP6300, Waltham, MA, USA) with the resolution of $\pm 5 \times 10^{-7}$. The total oxygen levels (T.[O]) of the steel samples were measured by inert gas fusion-infrared absorptiometry with the resolution of $\pm 10^{-6}$. The chemical compositions of all steel samples are given in Table 2. Another was polished for monitoring the inclusion properties, such as morphologies, size, and chemical compositions by scanning electron microscopy and energy dispersive spectroscopy (Zeiss Ultra-Plus, ZEISS, Jena, Germany). The size distribution of precipitates was surveyed in the observed regions of 19.86 mm^2, magnified 500× in the cross-section.

Table 2. The compositions of the obtained sample (mass %).

No.	[Al]	[Ca]	[Ti]	$a_{[O]}$	T.[O]
1-A	0.0042	-	0.0105	0.0005	0.0053
1-B	0.0036	0.0005	0.0094	-	0.0049
2-A	0.0053	-	0.0118	0.0006	0.0045
2-B	0.0051	0.0038	0.0115	-	0.0038
3-A	0.0430	-	0.0112	0.0002	0.0038
3-B	0.0413	0.0025	0.0106	-	0.0032

3. Results and Discussion

3.1. Chemical Composition, Size Distribution, and Morphologies of Inclusions

Titanium in the steel production process shows many valence states, such as Ti^{2+}, Ti^{3+}, and Ti^{4+} [43–45]. In addition, the types of titanium oxides are determined by combining the partial pressure of oxygen with mass fraction of titanium in steel [46]. Although a number of Ti-containing oxides (TiO, TiO_2, Ti_3O_5, Ti_2O_3, etc.) can exist as products of deoxidation reactions by titanium, when mass % Ti was between 0.0004 to 0.36, Ti_3O_5 was the only stable equilibrium oxide in steel, as demonstrated by the electron backscatter diffraction technique [43–46]. Based on the compositions of steel in the current research, the isothermal section of the Al_2O_3–Ti_3O_5–CaO ternary phase diagram at 1873 K with $p(O_2) = 10^{-14}$ atm (computed by FactSage 7.0, THERMFACT LTD, Quebec, Canada), as shown in Figure 3, was introduced to analyze the composition of inclusions. It can be easily seen from Figure 3 that solid phases (CaO, Ti_3O_5, Al_2O_3, perovskite, calcium aluminates, and titanium aluminates) coexist with liquid phases in the two- or three-phase zones. It is noticeable that two liquid phases emerge at 1873 K, which are locate in the regions with a small amount of CaO and Ti_3O_5.

The chemical elements, as well as mole ratios in each observed precipitate, were determined by SEM-EDS (Zeiss Ultra-Plus, ZEISS, Jena, Germany), and then the data were converted to mass fraction of CaO, Ti_3O_5, and Al_2O_3. As presented in Figure 4, each plot in the phase diagram represents an individual inclusion to assess inclusion behavior and transformation, and the thick red lines are liquiduses at 1873 K. As shown in Figure 4a, the inclusions in No.1 melt after Ti addition are mainly spherical titanium aluminates. There is no significant change in the morphologies of the inclusions after calcium treatment. Only a small amount of compositional changes occur in these inclusions which are still in liquid phases. By contrast, a mass of irregular inclusions of Al–Ti–Ca–O system are generated in No. 2 melt as result of the increased mass fraction of 40 ppm [Ca] by calcium treatment. As the mass

fraction of CaO in these inclusions is significantly increased, the locations of inclusion compositions in the isothermal section diagram are beyond the liquid region. From the view of the phase types, they mostly locate in perovskite and $(CaO)_3 \cdot (TiO_x)_2$. When the mass fraction of [Al] was increased from 40 ppm to 400 ppm, almost no liquid inclusions are found in No. 3 melt. Compared with No. 1 and No. 2 melts, the locations of inclusion compositions in No. 3 melt are outside of the liquidus in the isothermal section before calcium treatment, and bring on the corresponding irregular appearance. However, inclusions are evolved to calcium aluminates of liquid state after calcium treatment.

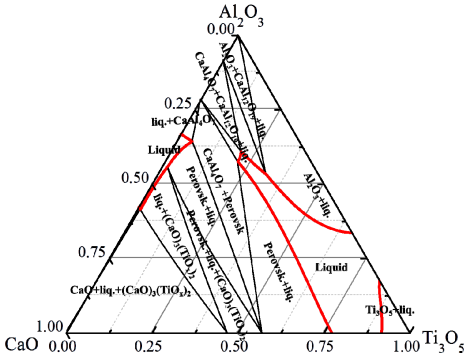

Figure 3. Isothermal section diagram of Ti_3O_5–Al_2O_3–CaO system at 1873 K with $p(O_2) = 10^{-14}$ atm.

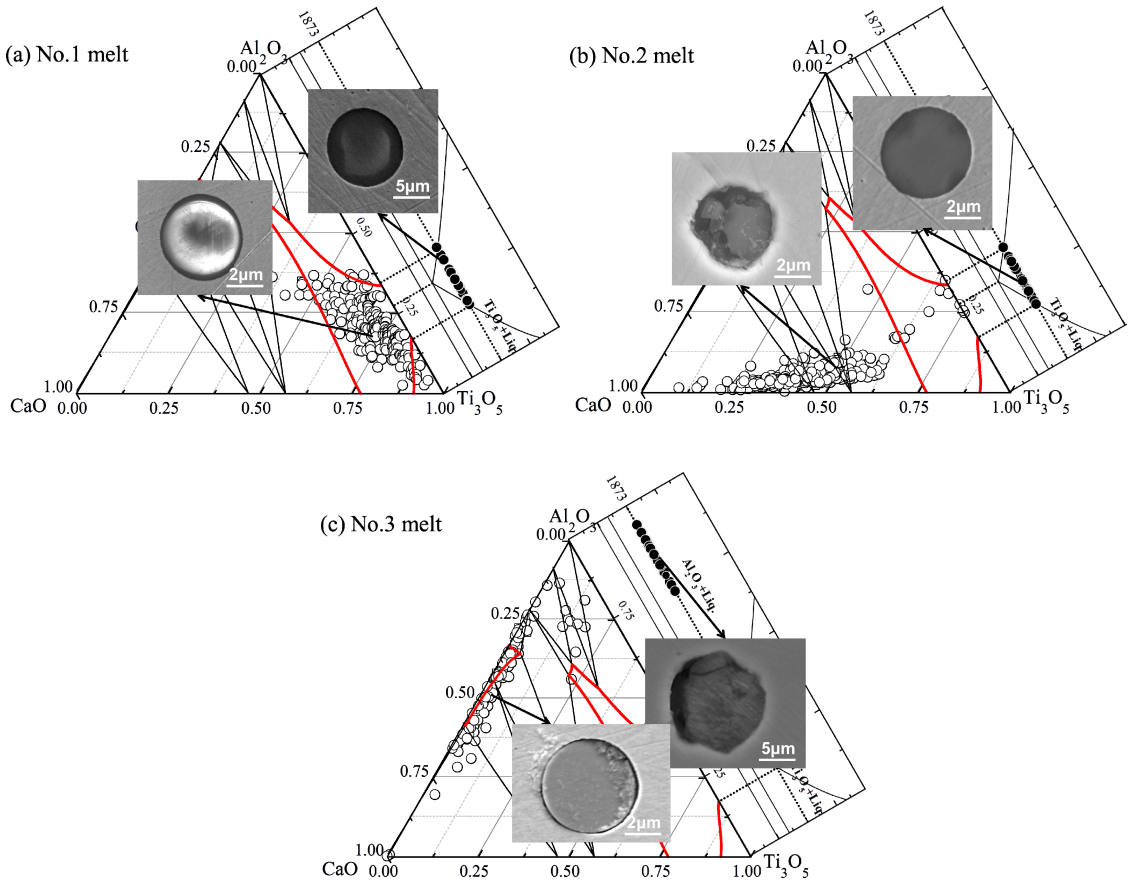

Figure 4. Morphologies and locations of inclusions in the isothermal sections. Thick red lines are the liquidus at 1873 K (1600 °C). The black plots represent the sample before calcium, and the white ones represent the sample after calcium. (**a**) No. 1 melt, (**b**) No. 2 melt, (**c**) No. 3 melt.

Figure 5 gives the size distributions of inclusions in the melts. The results indicate that more than half of the inclusions in sample 1-A are larger than 5 μm, and about 20% of the inclusions are smaller than 2 μm. There is no significant change in the size of inclusions after calcium treatment. There is just a little increase in the proportions of the larger inclusions (>10 μm) in sample 1-B. This may be due to collision and aggregation of the inclusions. The situation of No. 2 melt before calcium treatment is nearly identical to the former one. Nevertheless, the number of inclusions that are smaller than 5 μm in sample 2-B is more than 65%. This illustrates that the solid inclusions of Al_2O_3–CaO–TiO_x system trend to be fine and well-dispersed in the melts of Ti-bearing steel as treated by calcium. Apparently, the inclusions in sample 3-A also have a relatively small size. After calcium treatment, the proportion of the smaller inclusion in sample 3-B is obviously decreased and the numbers of inclusions are present as liquid state, combined with the results in Figure 4.

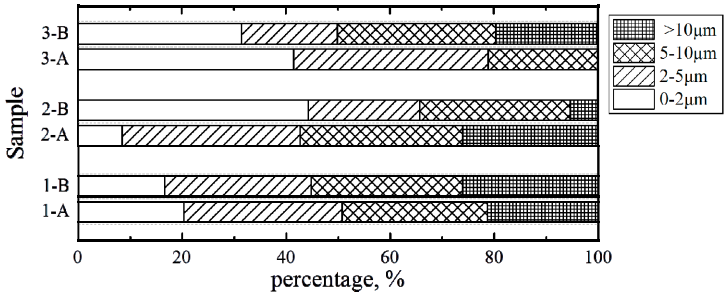

Figure 5. Size distributions of inclusions in all steel samples.

3.2. Thermodynamic Analysis of Al–Ti–Ca–O System

A series of generating reactions of inclusions, as listed in Table 2, were considered to understand the transformation process of Al–Ti–Ca–O system. The intermediate products, titanium oxides, CaO and calcium titanates in Table 3, could be firstly generated according to the very negative Gibbs energies of reactions between titanium/calcium and oxygen at 1873 K. As $12CaO{\cdot}7Al_2O_3$ is the only compound located inner of the liquidus in the phase diagrams of Al_2O_3–TiO_x and Al_2O_3–CaO–TiO_x systems at 1873 K, it is introduced as liquid calcium aluminate to calculate the equilibrium state with solid inclusions.

Table 3. Standard Gibbs energies of inclusions formation.

No.	Reactions	$\Delta G^\theta = A + B \times T$ /J·mol^{-1}		References
		A	*B*	
1	$Al_2O_3 = 2[Al] + 3[O]$	867,500	−222.5	[27]
2	$CaO = [Ca] + [O]$	138,227	63.0	[47]
3	$Al_2TiO_5 = [Ti] + 2[Al] + 5[O]$	1,435,000	−40.5	[23]
4	$CaO{\cdot}6Al_2O_3 = CaO_{(s)} + 6Al_2O_{3(s)}$	16,380	37.58	[48]
5	$CaO{\cdot}2Al_2O_3 = CaO_{(s)} + 2Al_2O_{3(s)}$	15,650	25.82	[48]
6	$CaO{\cdot}Al_2O_3 = CaO_{(s)} + Al_2O_{3(s)}$	17,910	17.38	[48]
7	$12CaO{\cdot}7Al_2O_3 = 12CaO_{(s)} + 7Al_2O_{3(s)}$	−618,000	612.1	[49]
8	$Ti_2O_3 = 2[Ti] + 3[O]$	822,000	−247.7	[50]
9	$Ti_3O_5 = 3[Ti] + 5[O]$	1,307,000	−381.8	[50]
10	$TiO_2 = [Ti] + 2[O]$	−675,600	234	[51]
11	$3CaO{\cdot}Ti_2O_3 = 3CaO_{(s)} + Ti_2O_{3(s)}$	192,745 (1873K)		[52]
12	$3CaO{\cdot}2TiO_2 = 3CaO_{(s)} + 2TiO_{2(s)}$	148,365	24.14	[52]
13	$CaO{\cdot}TiO_2 = CaO_{(s)} + TiO_{2(s)}$	74,392	10.13	[53]

The phase equilibrium calculations are based on the minimum Δ*G* theory, since the elements (such as Ca, Ti, Al, etc.) involved in the present research are of low concentration in molten steel. Therefore, the molten steel can be assumed to be an ideal solution and to follow Henry's law. The component activity coefficient was calculated by using 1% (mass) extremely dilute solution

as the standard state. The activity coefficient between the contents of all elements and the interaction coefficient (shown in Table 4) was expressed by Wagner's formula, as shown in Formula (1).

$$\log f_i = \sum_{j=2}^{n} e_i^j[\%j] + \sum_{j=2}^{n} r_i^j[\%j] + \sum_{j=2}^{n}\sum_{k=2}^{n} r_i^{j,k}[\%j][\%k] \quad (1)$$

Table 4. The interaction coefficients of Fe–Al–Ti–Ca–O system molten steel at 1873 K [54–69].

i	j	k	e_i^j	r_i^j	$r_i^{(j,K)}$	i	j	k	e_i^j	r_i^j	$r_i^{(j,K)}$
O	Al	Ca	−3.9	−0.01	0	Al	Al	O	0.043	−0.001	−0.028
		Ti			-		Ca	O	−0.047	0	0
		O			47.45		Ti	-	0.004	-	-
	Ca	Al	−310	−17,984	0		O	Al	−1.98	39.82	−0.028
		O			519,903			Ca			0
	Ti	O	−0.34	0.031	0.026	Ca	Al	-	−0.072	0.0007	-
	O	Al	−0.20	0	47.45		Ca	O	−0.002	-	−90,227
		Ca			520,000		Ti	-	−0.13	-	-
Ti	Al	-	0.0037	-	-		O	Ca	−580	650,129	−90,056
	Ti	O	0.042	−0.001	0.20	-					
	O	Ti	−3.4	−0.0355	0.20						

According to the activity of all elements and the free energy change for stable oxides' region transformation, the phase diagrams can be calculated, and the details of the calculation methods are mentioned in other work and my former work [70,71]. The phase diagrams involving Al–Ti–Ca–O system at 1873 K were worked out to estimate potential oxides in molten steel, and are shown in Figure 6. It can be seen from Figure 6a that CaO and CT ($3CaO{\cdot}2TiO_2$, $3CaO{\cdot}Ti_2O_3$, $CaO{\cdot}TiO_2$) are the main inclusions in the molten steel, as the mass fraction of calcium and titanium increase from 10^{-5}% to 10^{-2}%, and 10^{-4}% to 1%, respectively. When 0.005% aluminum is added into the Ca–Ti–O system as shown in Figure 6b, LCA (liquid calcium aluminate) precipitates, which squeezes the region of CT. It is obvious that aluminum content in steel has an important influence on stable phases of inclusions. As the mass fraction of aluminum increases to 0.05%, SCA (solid calcium aluminate) is present, which results in the further reduction of CT region, as shown in Figure 6c. It is noticeable that the stability region of liquid calcium aluminate is located in a common calcium content range. As the compositions of the steel samples in the current work (based on the content of the calcium and titanium) and experimental results introduced from Seo and Zheng [38,39] were marked in the phase diagrams, a good consistency in the above data is conspicuous, as shown in Figure 6b,c. Consequently, the calculated phase diagrams of Al–Ca–Ti–O system are reliable for effectively estimating the evolution behavior of inclusions at steelmaking temperature.

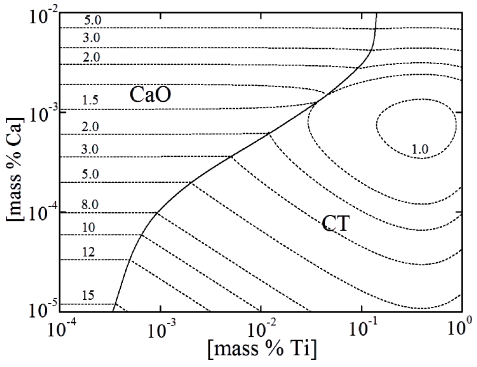

(a) Stability diagram of Ti-Ca-O system at 1873K

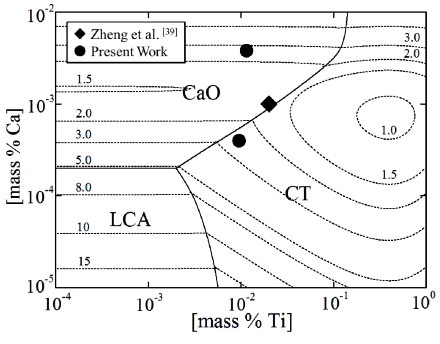

(b) Stability diagram of Al-Ti-Ca-O system at 1873K for [Al]=0.005 pct with experimental data

Figure 6. *Cont.*

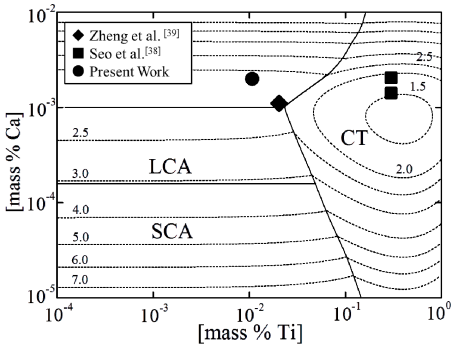

(c) Stability diagram of Al-Ti-Ca-O system at 1873K for [Al]=0.05 pct with experimental data

Figure 6. Calculated diagrams of stable oxides in the Al–Ca–Ti–O system at 1873 K (**a**) [Al] = 0, (**b**) [Al] = 0.005%, (**c**) [Al] = 0.05%.

Some transformation behaviors of precipitates are overlooked in this work, due to the extreme cooling speed during the sampling process. For this reason, the phase transformation of inclusions during solidification of melts was computed by FactSage 7.0 as the FSstel, FactPS, and FToxid databases were employed, and the relevant results are present in Figure 7. The mass fraction of aluminum and calcium varies in the Fe–Al–Ca–0.01Ti–0.005O systems when temperature decreases from 1873 K to 1473 K. It can be seen from Figure 7a that liquid inclusions are present in the steel at a wide temperature range, from 1873 K to about 1623 K, when the mass fractions of aluminum and calcium are both small, around 0.005%, and the transformation process follows liquid inclusions $\rightarrow Al_2O_3 \rightarrow 2CaO{\cdot}Ti_2O_3 \rightarrow Ti_2O_3$ during solidification. Nevertheless, the liquid inclusions only exist around 1873 K as the mass fraction of calcium increases to 0.003% and the formation of solid calcium titanates is favorable, as shown in Figure 7b. As the mass fraction of aluminum increases to 0.03%, while that of calcium is 0.005%, only alumina and calcium aluminates precipitate at 1873 K and no other inclusions are formed during the cooling process, as shown in Figure 7c. However, the liquid phase appears again at a higher temperature as the mass fraction of calcium increases 0.003% in Figure 7d. The liquid inclusions are modified into solid calcium aluminates during the solidification process. When the mass fraction of calcium increases further to 0.007%, the main stable phases become CaO and solid calcium titanates in steel, replacing the calcium aluminates as shown in Figure 7e.

From the found inclusions of Al–Ti–Ca–O system and the above thermodynamic analysis, it is suggested that the calcium treatment technique associated with the right aluminum addition is available to get the liquid phase inclusions at the casting temperature. The calcium addition needs to be reconsidered as the amount of aluminum varies in the steelmaking process.

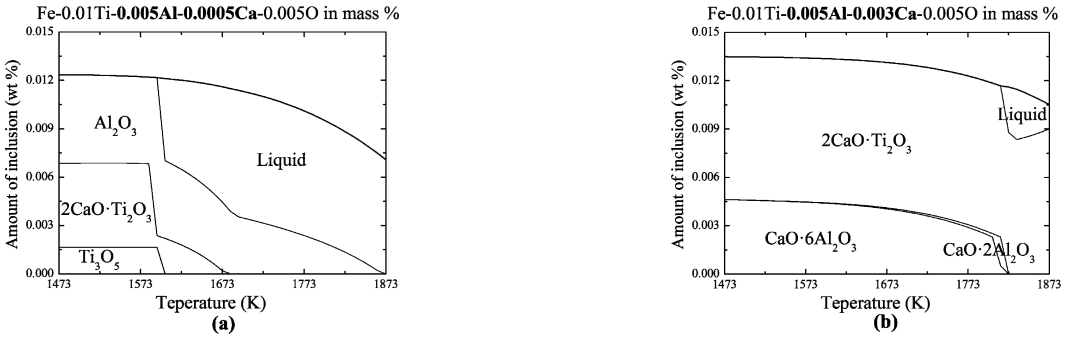

Figure 7. *Cont.*

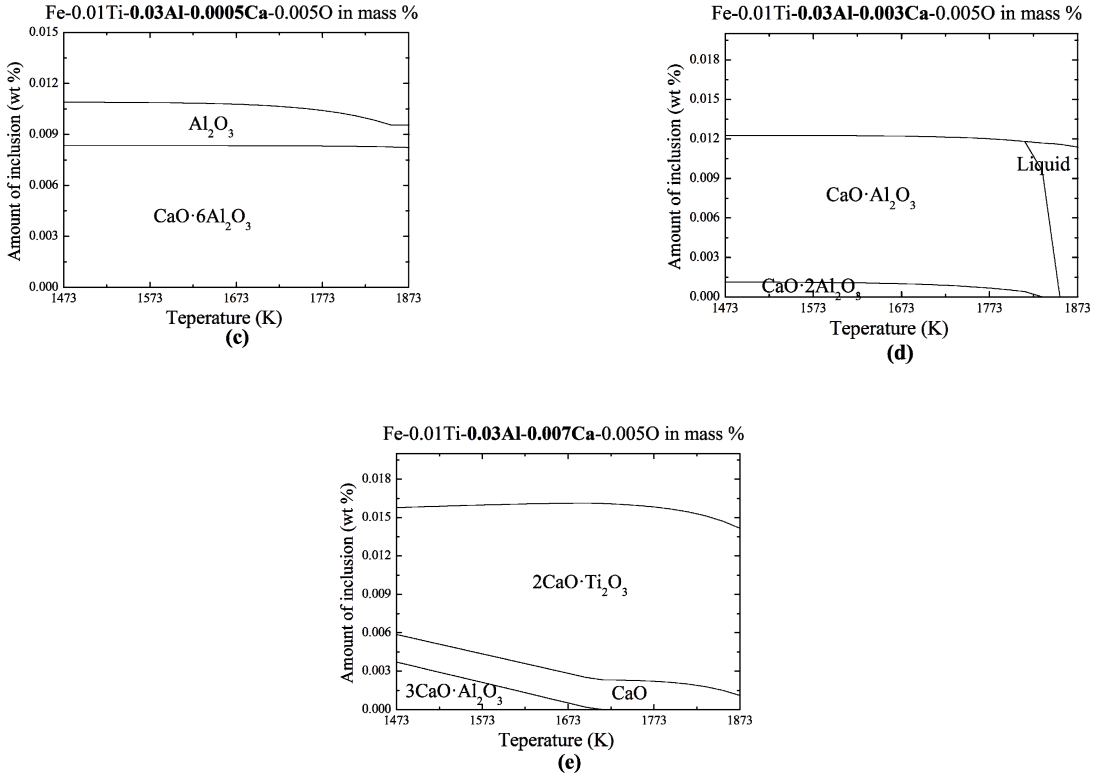

Figure 7. Transformation of inclusions during solidification as different compositions of steel. (**a**) [Al] = 0.005%, [Ca] = 0.0005%; (**b**) [Al] = 0.005%, [Ca] = 0.003%; (**c**) [Al] = 0.03%, [Ca] = 0.0005%; (**d**) [Al] = 0.03%, [Ca] = 0.003%; (**e**) [Al] = 0.03%, [Ca] = 0.007%.

4. Conclusions

The characteristics and transformation behaviors of the inclusions in Ti-containing steel after calcium addition with different aluminum amount have been discussed by physical simulations and thermodynamic analysis at 1873 K (1600 °C), as well as during solidification. The main results are summarized as follows.

The morphologies, chemical compositions, and size distribution of the inclusions are dramatically different before and after calcium treatment, and the calcium addition should be reconsidered according to the mass fraction of aluminum in order to get liquid phase inclusions. The generation of liquid inclusions is more favorable as less calcium addition is needed at the lower amount of aluminum, and as more calcium is appropriate for a higher amount of aluminum. That is, 0.0005% calcium for 0.0036% aluminum, and 0.0025% calcium for 0.0413% aluminum in this study. The inappropriate calcium treatment level can induce the generating trend of solid inclusions in melts. The inclusion-oriented diagrams of Al–Ti–Ca–O system in melts at 1873 K, and the transformation behaviors of inclusions during solidification of steel, were systemically computed involving all types of solid inclusions and liquid phases. The thermodynamic equilibrium calculations are in good agreement with experimental data, and the liquid inclusions can exist during the whole cooling process, as formed at steelmaking temperature.

Author Contributions: Conceptualization, Methodology, T.Z.; Writing—review & editing, Y.L., T.Z. and H.D., Funding Acquisition, T.Z. and Y.L.

Funding: Natural Science Foundation of Chongqing (cstc2018jcyjAX0792) and the Introduce Talents Research Start-up Fund in Central South University of China.

Conflicts of Interest: The authors declare no conflict of interest.

References

1. Liu, H.; Wang, H.; Li, L.; Zheng, J.; Li, Y.; Zeng, X. Investigation of Ti inclusions in wire cord steel. *Ironmak. Steelmak.* **2011**, *38*, 53–58. [CrossRef]
2. Liu, T.; Chen, L.; Bi, H.; Che, X. Effect of Mo on high-temperature fatigue behavior of 15CrNbTi ferritic stainless steel. *Acta Metall. Sin.* **2014**, *27*, 452–456. [CrossRef]
3. Zhang, J.; Cao, Y.; Jiang, G.; Di, H. Effect of annealing temperature on the precipitation behavior and texture evolution in a warm rolled P-containing interstitial-free high strength steel. *Acta Metall. Sin.* **2014**, *27*, 395–400. [CrossRef]
4. Lee, Y.D.; Park, S.H. Effects of titanium and niobium on the weldability of 11% Cr ferritic stainless steel. *J. Korean Inst. Met. Mater.* **1993**, *31*, 984–987.
5. Kim, H.S.; Chang, C.-H.; Lee, H.-G. Evolution of inclusions and resultant microstructural change with Mg addition in Mn/Si/Ti deoxidized steels. *Scr. Mater.* **2005**, *53*, 1253–1258. [CrossRef]
6. Wang, C.; Misra, R.; Shi, M.; Zhang, P.; Wang, Z.; Zhu, F.; Wang, G. Transformation behavior of a Ti–Zr deoxidized steel: Microstructure and toughness of simulated coarse grain heat affected zone. *Mater. Sci. Eng. A* **2014**, *594*, 218–228. [CrossRef]
7. Nakai, K.; Yudate, A.; Kobayashi, S.; Hamada, M.; Komizo, Y. Effects of Ti-based oxide inclusions on formation of intragranular ferrite in steel. *Tetsu-to-Hagané* **2004**, *90*, 141–145. [CrossRef]
8. Kiviö, M.; Holappa, L.; Iung, T. Addition of dispersoid titanium oxide inclusions in steel and their influence on grain refinement. *Metall. Mater. Trans. B* **2010**, *41*, 1194–1204. [CrossRef]
9. Kiviö, M.; Holappa, L. Addition of titanium oxide inclusions into liquid steel to control nonmetallic inclusions. *Metall. Mater. Trans. B* **2012**, *43*, 233–240. [CrossRef]
10. Wang, C.; Verma, N.; Kwon, Y.; Tiekink, W.; Kikuchi, N.; Sridhar, S. A study on the transient inclusion evolution during reoxidation of a Fe-Al-Ti-O melt. *ISIJ Int.* **2011**, *51*, 375–381. [CrossRef]
11. Wang, C.; Nuhfer, N.T.; Sridhar, S. Transient behavior of inclusion chemistry, shape, and structure in Fe-Al-Ti-O melts: Effect of titanium/aluminum ratio. *Metall. Mater. Trans. B* **2009**, *40*, 1022–1034. [CrossRef]
12. Wang, C.; Nuhfer, N.T.; Sridhar, S. Transient behavior of inclusion chemistry, shape, and structure in Fe-Al-Ti-O melts: Effect of titanium source and laboratory deoxidation simulation. *Metall. Mater. Trans. B* **2009**, *40*, 1005–1021. [CrossRef]
13. Zhang, T.; Liu, C.; Jiang, M. Effect of Mg on behavior and particle size of inclusions in Al-Ti deoxidized molten steel. *Metall. Mater. Trans. B* **2016**, *47*, 2253–2262. [CrossRef]
14. Wang, D.; Jiang, M.; Matsuura, H.; Tsukihashi, F. Dynamic evolution of inclusions in Ti-bearing Al-deoxidized molten irons at 1873 K. *Steel Res. Int.* **2014**, *85*, 16–25. [CrossRef]
15. Basu, S.; Choudhary, S.K.; Narendra, U. Nozzle Clogging Behaviour of Ti-bearing Al-killed Ultra Low Carbon Steel. *ISIJ Int.* **2004**, *44*, 1653–1660. [CrossRef]
16. Kawashima, Y.; Nagata, Y.; Shinme, K. Influence of Ti concentration on nozzle clogging on Al-Ti deoxidation: behavior of inclusion on Al-Ti deoxidation-2. *CAMP-ISIJ* **1991**, *4*, 1237–1242.
17. Jung, I.H.; Eriksson, G.; Wu, P.; Pelton, A. Thermodynamic modeling of the Al_2O_3-Ti_2O_3-TiO_2 system and its applications to the FeAl-Ti-O inclusion diagram. *ISIJ Int.* **2009**, *49*, 1290–1297. [CrossRef]
18. Ruby-Meyer, F.; Lehmann, J.; Gaye, H. Thermodynamic analysis of inclusions in Ti-deoxidised steels. *Scand. J. Metall.* **2000**, *29*, 206–212. [CrossRef]
19. Park, D.-C.; Jung, I.-H.; Rhee, P.C.H.; Lee, H.-G. Reoxidation of Al-Ti containing steels by CaO-Al_2O_3-MgO-SiO_2 slag. *ISIJ Int.* **2004**, *44*, 1669–1678. [CrossRef]
20. Doo, W.-C.; Kim, D.-Y.; Kang, S.-C.; Yi, K.-W. Measurement of the 2-dimensional fractal dimensions of alumina clusters formed in an ultra low carbon steel melt during RH process. *ISIJ Int.* **2007**, *13*, 249–258. [CrossRef]
21. Zinngrebe, E.; Van Hoek, C.; Visser, H.; Westendorp, A.; Jung, I.-H. Inclusion population evolution in Ti-alloyed Al-killed steel during secondary steelmaking process. *ISIJ Int.* **2012**, *52*, 52–61. [CrossRef]
22. Van Ende, M.-A.; Guo, M.; Dekkers, R.; Burty, M.; Van Dyck, J.; Jones, P.; Blanpain, B.; Wollants, P. Formation and evolution of Al-Ti oxide inclusions during secondary steel refining. *ISIJ Int.* **2009**, *49*, 1133–1140. [CrossRef]
23. Matsuura, H.; Wang, C.; Wen, G.; Sridhar, S. The transient stages of inclusion evolution during Al and/or Ti additions to molten iron. *ISIJ Int.* **2007**, *47*, 1265–1274. [CrossRef]

24. Seo, M.-D.; Cho, J.-W.; Kim, K.-C.; Kim, S.-H. Evolution of nonmetallic inclusions in ultra low carbon steel after aluminum deoxidization. *ISIJ Int.* **2014**, *54*, 475–481. [CrossRef]
25. Wu, Z.; Zheng, W.; Li, G.; Matsuura, H.; Tsukihashi, F. Effect of inclusions' behavior on the microstructure in Al-Ti deoxidized and magnesium-treated steel with different aluminum contents. *Metall. Mater. Trans. B* **2015**, *46*, 1226–1241. [CrossRef]
26. Wang, C.; Nuhfer, N.T.; Sridhar, S. Transient behavior of inclusion chemistry, shape, and structure in Fe-Al-Ti-O melts: Effect of gradual increase in Ti. *Metall. Mater. Trans. B* **2010**, *41*, 1084–1094. [CrossRef]
27. Itoh, H.; Hino, M. Assessment of Al deoxidation equilibrium in liquid iron. *Tetsu-to-Hagané* **1997**, *83*, 773–778. [CrossRef]
28. Zhang, L.; Thomas, B.G. State of the art in evaluation and control of steel cleanliness. *ISIJ Int.* **2003**, *43*, 271–291. [CrossRef]
29. Park, J.H.; Todoroki, H. Control of MgO Al_2O_3 Spinel Inclusions in stainless steels. *ISIJ Int.* **2010**, *50*, 1333–1346. [CrossRef]
30. Jung, I.H. Overview of the applications of thermodynamic databases to steelmaking processes. *Calphad* **2010**, *34*, 332–362. [CrossRef]
31. Taguchi, K.; Ono-nakazato, H.; Usui, T.; Marukawa, K.; Katogi, K.; Kpsaka, H. Complex deoxidation equilibria of molten iron by aluminum and calcium. *ISIJ Int.* **2005**, *45*, 1572–1576. [CrossRef]
32. Kurayasu, H.; Takayama, T.; Hinotani, S.; Shirota, Y. Phase analysis of Ca-containing inclusions in Ca-treated steels. *Tetsu-to-Hagané* **1996**, *82*, 1017–1022. [CrossRef]
33. Herrera, M.; Castro, F.; Castro, M.; Méndez, M.; Solís, H.; Castellá, A.; Barbaro, M. Modification of Al_2O_3 inclusions in medium carbon aluminium killed steels by AlCaFe additions. *Ironmak. Steelmak.* **2006**, *33*, 45–51. [CrossRef]
34. Blah, C.; Espérance, G.L.; LeHuy, H.; Forget, C. Development of an integrated method for fully characterizing multiphase inclusions and its application to calcium-treated steels. *Mater. Charact.* **1997**, *38*, 25–37.
35. Holappa, L.; Hämäläinen, M.; Liukkonen, M.; Lind, M. Thermodynamic examination of inclusion modification and precipitation from calcium treatment to solidified steel. *Ironmak. Steelmak.* **2003**, *30*, 111–115. [CrossRef]
36. Lind, M.; Holappa, L. Transformation of alumina inclusions by calcium treatment. *Metall. Mater. Tran. B* **2010**, *41*, 359–366. [CrossRef]
37. Zhang, T.; Min, Y.; Liu, C.; Jiang, M. Effect of Mg addition on the evolution of inclusions in Al–Ca deoxidized melts. *ISIJ Int.* **2015**, *55*, 1541–1548. [CrossRef]
38. Seo, C.-W.; Kim, S.-H.; Jo, S.-K.; Suk, M.-O.; Byun, S.-M. Modification and minimization of spinel (Al_2O_3·xMgO) inclusions formed in Ti-added steel melts. *Metall. Mater. Trans. B* **2010**, *41*, 790–797. [CrossRef]
39. Zheng, W.; Wu, Z.; Li, G.; Zhang, Z.; Zhu, C. Effect of Al content on the characteristics of inclusions in Al–Ti complex deoxidized steel with calcium treatment. *ISIJ Int.* **2014**, *54*, 1355–1364. [CrossRef]
40. Mizoguchi, T.; Ueshima, Y. Determination of the Ti_2O_3-CaO-Al_2O_3 phase diagram at steelmaking Temperature. *Tetsu-to-Hagané* **2005**, *91*, 376–382. [CrossRef]
41. Kim, K.-H.; Do, K.-H.; Choi, W.-J.; Lee, S.-B.; Kim, D.-S.; Pak, J.-J. Inclusion modification by Al deoxidation and Ca treatment in Ti containing 18%Cr stainless steel melts. *Korean J. Met. Mater.* **2013**, *51*, 113–118.
42. Zheng, H.; Chen, W. Formation of CaO·TiO_2-MgO·Al_2O_3 dual phase inclusion in Ti stabilized stainless steel. *J. Univ. Sci. Technol. B* **2006**, *13*, 16–20. [CrossRef]
43. Pak, J.-J.; Jo, J.-O.; Kim, S.-I.; Kim, W.-Y.; Chung, T.-I.; Seo, S.-M.; Park, J.-H.; Kim, D.-S. Thermodynamics of titanium and oxygen dissolved in liquid iron equilibrated with titanium oxides. *ISIJ Int.* **2007**, *47*, 16–24. [CrossRef]
44. Cha, W.-Y.; Miki, T.; Sasaki, Y.; Hino, M. Identification of titanium oxide phases equilibrated with liquid Fe-Ti alloy based on EBSD analysis. *ISIJ Int.* **2006**, *46*, 987–995. [CrossRef]
45. Cha, W.-Y.; Nagasaka, T.; Miki, T.; Sasaki, Y.; Hino, M. Equilibrium between titanium and oxygen in liquid Fe-Ti alloy coexisted with titanium oxides at 1873 K. *ISIJ Int.* **2006**, *46*, 996–1005. [CrossRef]
46. Seok, S.-H.; Miki, T.; Hino, M. Equilibrium between Ti and O in Molten Fe-Ni, Fe-Cr and Fe-Cr-Ni Alloys Equilibrated with 'Ti_3O_5' Solid Solution. *ISIJ Int.* **2011**, *51*, 566–572. [CrossRef]
47. Itoh, H.; Hino, M.; Ban-ya, S. Deoxidation equilibrium of calcium in liquid iron. *Tetsu-to-Hagané* **1997**, *83*, 695–700. [CrossRef]

48. Nagata, K.; Tanabe, J.; Goto, K.S. Standard free energies of formation of CaO-Al_2O_3 intermediate compounds by means of EMF measurement of galvanic cells. *Tetsu-to-Hagané* **1989**, *75*, 2013–2030. [CrossRef]
49. Yang, W.; Zhang, L.; Wang, X.; Ren, Y.; Liu, X.; Shan, Q. Characteristics of inclusions in low carbon Al-killed steel during ladle furnace refining and calcium treatment. *ISIJ Int.* **2013**, *53*, 1401–1410. [CrossRef]
50. Cha, W.-Y.; Miki, T.; Sasaki, Y.; Hino, M. Temperature dependence of Ti deoxidation equilibria of liquid iron in coexistence with 'Ti_3O_5' and Ti_2O_3. *ISIJ Int.* **2008**, *48*, 729–738. [CrossRef]
51. Hong, T.; Debroy, T. Time-temperature-transformation diagrams for the growth and dissolution of inclusions in liquid steels. *Scr. Mater.* **2001**, *44*, 847–852. [CrossRef]
52. The Japan Society for the Promotion of Science. *Steelmaking Data Sourcebook*; Gordon and Breach Science Publishers: New York, NY, USA, 1988.
53. Chen, J. *Handbook of Data on Steelmaking*, 2nd ed.; Metallurgical Industry Press: Beijing, China, 2010.
54. Kishi, M.; Inoue, R.; Suito, H. Thermodynamics of oxygen and nitrogen in liquid Fe-20 mass% Cr alloy equilibrated with titania based slags. *ISIJ Int.* **1994**, *34*, 859–867. [CrossRef]
55. Ohta, M.; Morita, K. Thermodynamics of the MnO-Al_2O_3-TiO_2 system. *ISIJ Int.* **1999**, *39*, 1231–1238. [CrossRef]
56. Morioka, Y.; Morita, K.; Tsukihashi, F.; Sano, N. Equilibria between molten steels and inclusions during deoxidation by titanium-manganese alloy. *Tetsu-to-Hagané* **1995**, *81*, 40–45. [CrossRef]
57. Karasev, A.; Suito, H. Analysis of size distributions of primary oxide inclusions in Fe-10 mass Pct Ni-M (M = Si, Ti, Al, Zr, and Ce) alloy. *Metall. Mater. Trans. B* **1999**, *30*, 149–157. [CrossRef]
58. Ohta, M.; Morita, K. Thermodynamics of the Al_2O_3-SiO_2-TiOX oxide system at 1873 K. *ISIJ Int.* **2002**, *42*, 474–481. [CrossRef]
59. Ma, Z.; Janke, D. Characteristics of oxide precipitation and growth during solidification of deoxidized steel. *ISIJ Int.* **1998**, *38*, 46–52. [CrossRef]
60. Cho, S.W.; Suito, H. Assessment of Aluminum-Oxygen equilibrium in liquid iron and activities in CaO-Al_2O_3-SiO_2 slags. *ISIJ Int.* **1994**, *34*, 177–185. [CrossRef]
61. Taguchi, K.; Ono-nakazato, H.; Nakai, D.; Usui, T.; Marukawa, K. Deoxidation and desulfurization equilibria of liquid iron by calcium. *ISIJ Int.* **2003**, *43*, 1705–1709. [CrossRef]
62. Itoh, H.; Hino, M. Thermodynamics on the formation of spinel nonmetallic inclusion in liquid steel. *Metall. Mater. Trans. B* **1997**, *28*, 953–956. [CrossRef]
63. Jo, S.K.; Song, B. Thermodynamics on the formation of spinel ($MgO{\cdot}Al_2O_3$) inclusion in liquid iron containing Chromium. *Metall. Mater. Trans. B* **2002**, *33*, 703–709. [CrossRef]
64. Ishii, F.; Ban-ya, S. Thermodynamics of the deoxidation equilibrium of aluminum in liquid nickel and Nickel-Iron alloys. *ISIJ Int.* **1996**, *36*, 25–31. [CrossRef]
65. Higuchi, Y.; Numata, M. Effect of method of Ca treatment on composition and shape of non-metallic inclusions. *Tetsu-to-Hagané* **1996**, *82*, 671–676. [CrossRef]
66. Ohta, H.; Suito, H. Activities in CaO-MgO-Al_2O_3 slags and deoxidation equilibria of Al, Mg, and Ca. *ISIJ Int.* **1996**, *36*, 983–990. [CrossRef]
67. Itoh, H.; Hino, M. Thermodynamics on the formation of nonmetallic inclusion of spinel ($MgO{\cdot}Al_2O_3$) in liquid steel. *Tetsu-to-Hagané* **1998**, *84*, 85–90. [CrossRef]
68. Satoh, N.; Taniguchi, T. Prediction of nonmetallic inclusion formation in Fe-40mass% Ni-5mass% Cr alloy production process. *Tetsu-to-Hagané* **2009**, *95*, 827–836. [CrossRef]
69. Cho, S.W.; Suito, H. Assessment of calcium-oxygen equilibrium in liquid iron. *ISIJ Int.* **1994**, *34*, 265–269. [CrossRef]
70. Zhang, T.; Wang, D.; Jiang, M. Effect of Magnesium on the Evolution of Oxide and Sulphide in Liquid Iron at 1873K. *J. Iron Steel Res. Int.* **2014**, *21*, 1073–1080. [CrossRef]
71. Zhang, L.; Ren, Y.; Duan, H.; Yang, W.; Sun, L. Stability Diagram of Mg-Al-O System Inclusions in Molten Steel Effect of Magnesium on the Evolution of Oxide and Sulphide in Liquid Iron at 1873K. *Metall. Mater. Trans. B* **2015**, *46*, 1809–1825. [CrossRef]

© 2019 by the authors. Licensee MDPI, Basel, Switzerland. This article is an open access article distributed under the terms and conditions of the Creative Commons Attribution (CC BY) license (http://creativecommons.org/licenses/by/4.0/).